Inclusive measurement of (p,π^-xn) double charge exchange reactions on bismuth from threshold to 800 MeV

M. Dombsky and J. M. D'Auria
Department of Chemistry, Simon Fraser University, Burnaby, British Columbia, Canada V5A 1S6

I. Kelson and A. I. Yavin
Department of Physics and Astronomy, Tel Aviv University, Tel-Aviv, Israel 69978

T. E. Ward
Indiana University, Bloomington, Indiana 47405

J. L. Clark*
Nuclear Chemistry Division, Los Alamos National Laboratory, Los Alamos, New Mexico 87545

T. Ruth and G. Sheffer
TRIUMF, Vancouver, British Columbia, Canada V6T 2A3
(Received 25 February 1985)

The energy dependence of the total angle-integrated cross section for the production of astatine isotopes from (p,π^-xn) double charge exchange reactions on bismuth (^{209}Bi) was measured from 120 to 800 MeV using activation and radiochemical techniques. Chemical yields were estimated by direct radioassaying of ^{211}At activity in thin (~ 1 mg/cm^2), irradiated bismuth targets. Calculations of the contributions of secondary (two-step) reactions to these measured astatine yields were performed, based partially upon the observed ^{211}At activity although even at the highest energies, the contribution to products lighter than ^{207}At was negligible. These data for products with as many as seven neutrons removed from the doubly coherent product (^{210}At) display nearly Gaussian shapes for the mass distributions of the astatine residues, with the maximum occurring for about ^{204}At. The most probable momentum transfer deduced from these distributions for the initial π^- production step was 335 MeV/c. The observed excitation functions display a behavior similar to that observed for the yield of ^{210}Po from a (p,π^0) reaction on ^{209}Bi, but radically different from that observed for inclusive π^- reactions on a heavy nucleus. These data are discussed in terms of recent theoretical approaches to negative pion production from bismuth. In addition, a simple, schematic model is developed to treat the rapidly decreasing percentage of the total inclusive π^- emission which is observed for this double charge exchange reaction. This model reflects the opacity of a nucleus to a source of internal energetic protons.

I. INTRODUCTION

The (p,π) reaction on nuclei has received much attention in recent years both experimentally and theoretically.[1-7] In general, most experiments study exclusive reactions to discrete states using magnetic spectrometers, and light to intermediate mass nuclei where individual nuclear states can be resolved. Recently, large cross sections for (p,π^-) transitions to some specific two-particle, one-hole states in light and medium weight nuclei were observed at the Indiana University Cyclotron Facility (IUCF).[8] In heavy nuclei, states are more closely spaced and inclusive reactions are usually studied.[9,10] Crawford *et al.*,[9] for example, studied inclusive cross sections for the (p,$\pi^\pm$) reaction at 585 MeV in a variety of targets, and for lead they measured a cross section of 41.51 mb for (p,π^-), while the cross section for (p,π^+) was higher by a factor of 2. There is little data, however, on the energy dependence of the total cross section for the (p,π) or specifically (p,π^-) reaction on nuclei. In free nucleon-nucleon collisions the cross section for pion production was found to increase steeply with energy below 600 MeV. For the inclusive differential cross section, Krasonov *et al.*[11] showed that for copper, $d\sigma/d\Omega$ (90°) rises steeply with energy below 500 MeV. Clearly it is of some importance to the understanding of pion production in nucleon-nucleus interactions to provide data on the energy dependence of such production in nuclei. The recent study by Julien *et al.*,[12] suggesting the possibility of resonance structure at $E_p = 350$ MeV in (p,π) inclusive studies, reflects the exciting opportunities for new insights. At low energy, i.e., near the threshold for pion production in nuclei (~ 140 MeV), the possibility exists to study inclusive, double charge exchange (p,π^-) cross sections by activation and radiochemical approaches.

The present investigation was part of a systematic study of pion production[13] and charge exchange[14] on bismuth using intermediate energy protons at IUCF, TRIUMF, and the Los Alamos Meson Physics Facility (LAMPF). The use of activation and radiochemical techniques allows several unique opportunities. First, it allows one to identi-

fy individual isobaric mass residues which result from the (p,π) process. The coherent product of simple π^- emission, i.e., with no other emitted particle, can be separated from other products. Second, by combining data for all $(\pi^- xn)$ products one, in effect, has a measure of all double-charge exchange reactions leading to single π^- emission only, i.e., an inclusive type of measurement. Third, the observed isobaric mass distributions at different E_p yield information about the original excitation spectrum resulting from the initial (p,π) process. The measured quantities of inclusive radiochemical studies are a sum of cross sections to all bound states of a residual nucleus and are devoid of nuclear structure influences of a particular state. The reaction mechanism is important and insights on the mechanism of pion production, inferred from its effects on the residual nucleus, could be gained. For example, Dillig calculated[13] the excitation function for the $^{209}Bi(p,\pi^0)^{210}Po$ reaction measured up to 480 MeV using a density of states factor, a two nucleon t matrix, and taking into account the initial states (proton) and final state (pion) distortions using optical potentials. This two-nucleon model (TNM) calculation reproduced the (p,π^0) data qualitatively, indicating a substantial contribution to the nuclear state density from weakly bound states. Furthermore, a moderate valley structure for $200 \leq E_p \leq 400$ MeV was reproduced qualitatively, indicating that pion distortions, in this case π absorption in the 3,3 resonance energy region, can have an effect. One can therefore infer information concerning the initial excitation energy and momentum transfer in inclusive $(p,\pi^- xn)$ cross sections and to estimate the relative isobaric yields of the doubly coherent (p,π) reactions to ^{210}Bi, ^{210}Po, and ^{210}At.

Clark *et al.*[15] have recently reported radiochemical results for the $^{209}Bi(p,\pi^- xn)^{210-x}At$ reaction at 200 MeV by observing the alpha and gamma activities of the astatine products. The sum of the cross sections measured was 48 ± 13 μb, which they suggest amounts to 90—95 % of the total inclusive double charge exchange (DCE) cross section at this energy. Evaporation calculations[15] indicated that only 5—10 % of the total DCE cross section would result from charge particle emission channels. There have been two theoretical attempts to understand the individual and sum cross sections for the $^{209}Bi(p,\pi^- xn)^{210-x}At$ reactions around 200 MeV. Gibbs[16] considered within the context of a TNM, the situation in which the (p,π^-) transition leaves the nucleus in a 2p1h state. He then assumed a simple quadratic form for the energy dependence of the density of states and predicted excitation functions for the individual, residual $^{210-x}At$ isotope over a limited energy range. His prediction agreed well with the measured distribution at 200 MeV. Long *et al.*, on the other hand, calculated[17] the sum cross section for the production of all isotopes up to 220 MeV using the intranuclear cascade (INC) approach. They assumed that three processes contribute to the reactions: direct (p,π^-) reaction on a target nucleon; (p,n) followed by (n,π^-); and (p,π^0) followed by (π^0,π^-). Good agreement with the data at 200 MeV was achieved, but the authors suggested that the agreement could be fortuitous.

In the present study the inclusive DCE reaction $^{209}Bi(p,\pi^- xn)^{210-x}At$ was investigated by detecting the astatine residual product activities. Total reaction cross sections from the production of At residues were measured from below threshold (120 MeV) up to 800 MeV using activation and radiochemical techniques. The cross sections for production of individual isotopes were also summed to allow an estimate of the inclusive DCE π^- production process and compared to the energy dependence of total inclusive π^- production. The rapidly diverging differences between these are discussed in terms of a schematic, cascade-based approach reflecting the opacity of the bismuth nucleus to low energy protons. From the residual isotopic distribution, information about the original excitation spectra and momentum transfer are also inferred.

II. EXPERIMENTAL PROCEDURE

Target irradiations were carried out at three facilities. Measurements at proton energies from 120 to 214 MeV were performed at the Indiana University Cyclotron Facility, from 188 to 481 MeV at the TRIUMF Cyclotron Facility (Vancouver, Canada), and at 800 MeV at the Clinton P. Anderson Meson Physics Facility at Los Alamos, New Mexico. Beam currents were 0.2—0.6 μA at IUCF, 1.5—3 μA at TRIUMF, and 2—3 μA at LAMPF. Irradiation times were 1—2 h at IUCF, ~1 h at TRIUMF, and from 10 min to 1 h at LAMPF. Beam integration at IUCF was measured with a Faraday cup, while at TRIUMF and LAMPF it was deduced from the ^{24}Na activity[18] produced in thin aluminum foils (1.85 mg/cm^2) of the same area as the target. For the TRIUMF and LAMPF measurements the target was made of a thin bismuth layer (0.8—2 mg/cm^2) evaporated onto thin aluminum backing. Due to the lower currents at IUCF, thick targets (10—45 mg/cm^2) had to be used. Very thick targets (100—1000 mg/cm^2) were also irradiated at several proton energies in order to study the contribution of secondary reactions to astatine production. Whereas secondary reactions are usually caused by alphas (and other particles) produced in the target, the LAMPF irradiations also contained contributions of secondary reactions from particles originating in air. The targets at IUCF and TRIUMF were irradiated in vacuum.

Astatine has no long-lived nuclides that can conveniently be used as tracers for the determination of the chemical separation efficiency.[19] A method was therefore developed which enabled us to determine the cross sections without reference to chemical yields. Two identical, thin targets were irradiated at each proton energy. The first (or "direct") target was put aside for several hours to allow for the short-lived activities to decay. The radioisotope ^{211}At, whose half-life is 7.2 h, is in secular equilibrium with its decay product ^{211}Po ($t_{1/2} = 0.52$ sec) which emits a distinct high energy alpha (7.45 MeV). The yield of these alphas is directly related to the production rate of ^{211}At, which in turn only arises from secondary reaction processes. (Any ^{211}Po which is produced from secondary processes that do not involve ^{211}At, decays away and is not counted.) The second target (labeled "separated") un-

derwent chemical separation[15,20] for astatine immediately after the irradiation. It was first dissolved in a minimum of concentrated HNO_3, with the excess nitrate neutralized by dropwise addition of $NH_2OH \cdot HCl$. The resulting solution was acidified to 8 *M* in HCl and the At^0 reduced to At^- with 1 *M* $SnCl_2$ in 8 *M* HCl. The reduced solution was loaded into a 10 cm long, 0.5 cm in diameter column containing 30 mesh Te metal. After successively washing the column with HCl and H_2O, the astatine was eluted with 2 ml of 2 *M* NaOH. The final solution was acidified to 1.5 *M* in HCl and the astatine spontaneously plated onto a silver foil. The resulting source, of approximately the same diameter as the beam spot on the direct target ($\sim$1 cm), was dried with methanol and counted for astatine activity. On the average, chemical separation and source preparation were completed within 40 min from the end of irradiation. Calculations based on observed ^{208}Po activity showed that at most 0.4% of the polonium produced passed through the separation.

The chemically separated astatine activities were determined by simultaneous alpha and gamma counting in a vacuum chamber with a thin aluminum window, allowing for the positioning of an external Ge(Li) detector as well as an internal Si surface-barrier detector. The detection efficiencies of the gamma detector were determined by calibration with ^{226}Ra and with commercially available standard reference sources. The solid angle subtended by the alpha detector was determined from a ^{208}Po source of the same geometry as the plated samples, cross calibrated with a standard ^{214}Am source. The characteristics[19] of the alpha and gamma activities used to identify the various At nuclides are given in Table I. ^{211}At, ^{204}At, and ^{203}At were identified by their half-lives and alpha energies, ^{210}At and ^{208}At by γ spectroscopy, and the other nuclides by both methods. Whenever possible, measurements were carried out by both systems and the degree of agreement was used to determine the reliability of the two systems. ^{210}At was also measured indirectly, by counting the alpha activity of the ^{210}Po daughter (after the ^{210}At had completely decayed). All gamma spectra were analyzed with the GAMANAL program,[21] and alpha spectra were integrated by hand. Figure 1 shows an alpha spectrum from a direct, irradiated target, labeled (a), and that from a chemically separated sample, labeled (b), both produced at $E_p = 399$ MeV.

In general, cross sections were determined in the following way. As mentioned above, ^{211}At can be produced only by secondary processes. Thus, we first calculated the effective cross section $\sigma_{eff}(^{211}\text{At})$ for the production of ^{211}At from the yield in the direct target [see Fig. 1(a)]. We then multiplied this effective cross section by the ratio of yields $^{210-x}\text{At}/^{211}\text{At}$ in the chemically separated target of the

TABLE I. Some decay characteristics of astatine isotopes. All values are from Ref. 19 except when indicated otherwise.

Nuclide	$t_{1/2}$	E_α (MeV)	Branching ratio (%)	E_γ (keV)	Branching ratio (%)	Q^c (MeV)
^{211}At	7.21 h	5.866	41.9			
		7.450[a]	57.2			
^{210}At	8.3 h			245.3	79.4	−138.6
				1181.4	99.3	
^{210}Po	138 d	5.304	99.9			
^{209}At	5.42 h	5.647	8.4[b]	545.0	94.4	−145.7
				781.9	86.6	
				790.2	66.0	
^{208}At	1.63 h			177	46.0	−154.1
				660	90.1	
				685	97.9	
^{207}At	1.81 h	5.759	11.5[b]	588.4	22	−161.5
				814.5	49	
^{206}At	31.4 min	5.703	0.96	395.5	47.8	−170.1
				477.1	85.9	
				700.7	97	
^{205}At	26.2 min	5.901	10	520.5	3.67	−178.0
				628.8	4.76	
				669.4	8.4	
				719.3	28	
^{204}At	9.3 min	5.948	4.4			−187.0
^{203}At	7.3 min	6.086	31			−195.1
^{202}At	3.0 min	6.227	15			−204.6
^{201}At	1.5 min	6.342	71			−212.7

[a]From decay of ^{211}Po daughter; $t_{1/2} = 0.525$ sec.
[b]From Ref. 15.
[c]From Ref. 44.

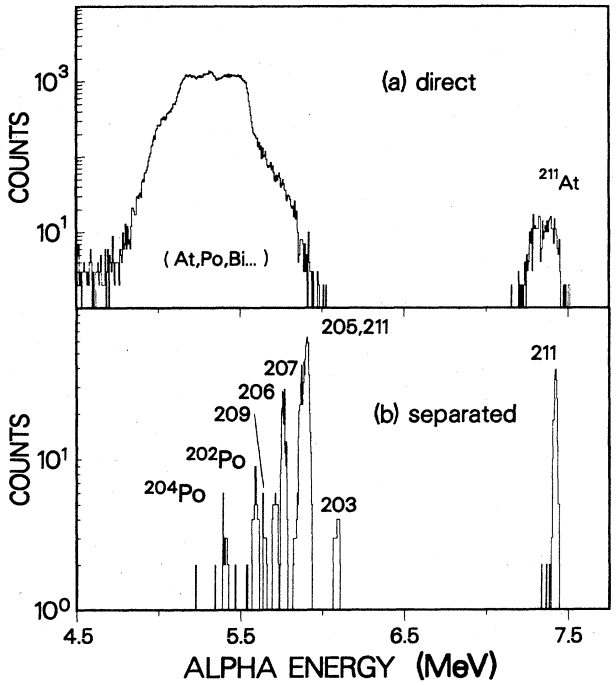

FIG. 1. Alpha spectra from the irradiation of ^{209}Bi by 399 MeV protons. (a) Thin (0.84 mg/cm^2) direct target itself; alpha peaks from At, Po, Bi, etc. (b) Chemically separated astatine target; alpha peaks from At isotopes as well as some Po contaminants.

same thickness [Fig. 1(b)], to get σ_x. Typically, the ratio error was about 20%, and for $\sigma_{\text{eff}}(^{211}\text{At})$ about 10%, although in some isolated cases the errors were larger. The error in the ratio resulted mainly from counting statistics, uncertainties in the literature branching ratios, and the relative calibration of the two counting systems. The error in $\sigma_{\text{eff}}(^{211}\text{At})$ included uncertainties in detection efficiency ($\approx$5%), beam integration ($\approx$7%), and target thickness ($\approx$6%). Uncertainties in counting statistics varied widely, from being as low as 1% for some high intensity gammas to values of $\approx$40% for some low intensity alphas and gammas. The loss of At activity due to recoiling out of the target for all At isotopes produced was determined to be less than 1.5%.

The determination of both cross sections and errors depended on our ability to calculate the production of ^{211}At and other At isotopes resulting from secondary processes. In addition to the primary reactions ^{209}Bi(p,$\pi^- x$n)$^{210-x}$At, astatine was also produced from a two-step process, namely ^{209}Bi+p$\rightarrow$He+$\cdots$, followed by ^{209}Bi(He,xn)At, where He stands for either an alpha or a ^{3}He ion. Similar reactions involving heavier ions such as lithium are expected to be insignificant, since (p,Li) producton is at most 1% of (p,α) production at the proton energies under consideration.[22,23] Production of astatine by protons on thick bismuth targets has previously been measured at Dubna[24–26] and Orsay[27–29] in the energy range 60–660 MeV; the astatine production was attributed to secondary production with intermediate alphas. However, Kurchatov *et al.*[24] noted that the light At nuclei ($A \leq 205$) could not be produced in quantity by secondary processes and attributed their formation to the primary (p,$\pi^- x$n) process. The thick target studies deduced the emitted alpha-energy distribution from measured yield ratios of At nuclides and known (α,xn) excitation functions. By reversing the calculation, we estimated the secondary production of astatine in our targets by combining the energy distribution of the α and ^{3}He ejectiles from (p,α) and (p,^{3}He) with the known excitation functions for bismuth of (α,xn) and (^{3}He,xn) reactions. Details of the calculations are given in the Appendix. The results of the calculations (see Fig. 2) show significant contribution to ^{210}At and ^{209}At production from secondary reactions involving alphas and ^{3}He ions. For ^{208}At and ^{207}At the secondary production was greatly reduced, and for the lighter nuclei it could be entirely ignored. In order to check the reliability of our estimates we compared the calculated values for the heavier At isotopes with the measured values at Dubna[21–26] and Orsay.[27–29] The agreement ranged from $\pm$4% for ^{210}At and ^{209}At to 30% for ^{208}At, once branching ratio corrections were made on the earlier data. The calculations also predicted well the measured ^{209}At and ^{207}At production yields observed in the present experiment at $E_p = 120$ MeV, an energy which is below the threshold for pion production.

III. EXPERIMENTAL RESULTS

The results of the cross section measurements are presented in Table II. The incident proton energy, E_p, is shown in the first column and the target thickness in the second column. The cross section for the production of ^{211}At as measured directly, i.e., without chemical separation [see Fig. 1(a)], is presented in the third column. It is labeled $\sigma_{\text{eff}}(^{211}\text{At})$ since it is produced only by secondary reactions. Yield ratios σ_x/σ_{211} for $x = 0,1,2,\ldots,7$, from the chemically separated targets [see Fig. 1(b)], are shown in columns 4–11. As mentioned earlier the cross section for the specific ^{209}Bi(p,$\pi^- x$n)$^{210-x}$At reaction is then ob-

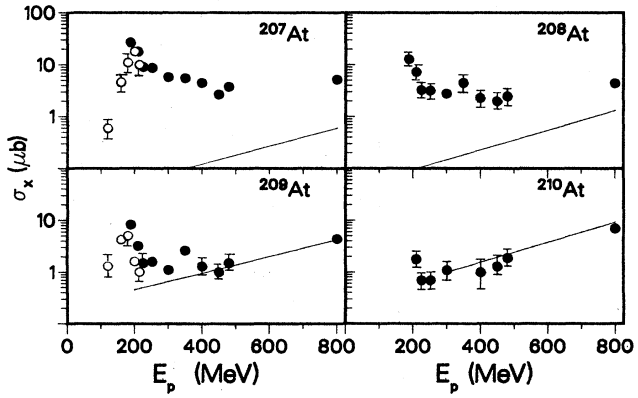

FIG. 2. Uncorrected data from IUCF (open circles), TRIUMF (filled), and LAMPF (filled), for the total production cross section including secondaries of the four heaviest $^{210-x}$At isotopes produced in the irradiation of Bi by protons. The solid line represents the calculated contribution from secondary reactions.

TABLE II. Cross section ratios for the ^{209}Bi(p,π^-x n)$^{210-x}$At reactions (including contribution from secondary reactions, see the text).

E_p	Target thickness (mg/cm^2±6%)	$\sigma_{eff}(^{211}At)$ (μb)	$\frac{\sigma_{210}}{\sigma_{211}}$	$\frac{\sigma_{209}}{\sigma_{211}}$	$\frac{\sigma_{208}}{\sigma_{211}}$	$\frac{\sigma_{207}}{\sigma_{211}}$	$\frac{\sigma_{206}}{\sigma_{211}}$	$\frac{\sigma_{205}}{\sigma_{211}}$	$\frac{\sigma_{204}}{\sigma_{211}}$	$\frac{\sigma_{203}}{\sigma_{211}}$
120	1000	6.0±1.5		0.3±0.1		0.2±0.1				
120	104	5.0±1.0		0.3±0.1		0.1±0.05				
160	46.1	4.6±0.9		0.9±0.3		1.0±0.3				
180	28.6	2.5±0.5		2.0±0.6		4.2±1.3				
188	1.01	1.3±0.2	<2	6.2±0.7	9.7±1.5	20 ±2	17 ±3			
200	36.2	3.9±0.8		0.4±0.1		4.5±1.4				
210	0.94	1.2±0.1	1.6±0.2	2.7±0.1	6.4±0.9	16 ±0.6	29 ±2	52 ±4	19 ±3	0.9±0.4
214	8.8	1.3±0.4		0.8±0.3		7.7±3.2				
225	1.10	1.1±0.1	0.7±0.2	1.5±0.1	2.9±0.4	7.9±0.3	15 ±1	39 ±3	20 ±4	12 ±3
252	1.13	1.5±0.2	0.6±0.1	1.1±0.1	2.2±0.4	6.0±0.3	15 ±1	34 ±4	20 ±4	32 ±5
300[a]	1.04	1.4±0.4	1.0±0.3	0.8±0.1	1.8±0.3	4.3±0.2	10 ±1	26 ±3	28 ±9	14 ±6
350	1.18	2.4±0.3		1.1±0.1	1.9±0.5	2.3±0.2	7 ±1	13 ±2	11 ±3	12 ±3
399	0.84	2.0±0.2	0.5±0.2	0.6±0.1	1.1±0.4	2.2±0.2	5.2±0.7	16 ±2	7.2±3.3	18 ±5
450	1.04	1.9±0.2	0.6±0.2	0.5±0.1	1.0±0.3	1.4±0.1	5.0±0.8	10 ±1		13 ±3
481	0.77	2.8±0.3	0.7±0.2	0.5±0.1	0.9±0.3	1.3±0.1	3.1±0.4	9 ±1	8.4±2.4	11 ±2
800[b]	0.4–2.0	10.0±0.4	0.7±0.05	0.4±0.01	0.4±0.03	0.5±0.01	0.8±0.03	2.4±0.1	2.0±0.3	2.9±0.3

[a]Average of 2 runs.
[b]Average of 7 runs.

tained by multiplying $\sigma_{\text{eff}}(^{211}\text{At})$ by the corresponding measured ratio of σ_x/σ_{211}. The values of the cross section for the four heaviest $^{210-x}$At isotopes are shown in Fig. 2. The solid circles are the measurements at TRIUMF and LAMPF, where thin targets were used. The open circles are the measurements at IUCF where thick targets were used. The solid line represents the calculated contribution from secondary reactions for a thin target. For the four lightest At isotopes, the contribution of secondary reactions to σ_x was negligible. The measured excitation functions for the eight observed $^{210-x}$At isotopes produced in the $(p,\pi^- xn)$ reaction (corrected for contributions from secondary reactions) are shown in Fig. 3. The open square is the value measured by Clark *et al.*[15] In each case, the arrow indicates the threshold for the production of the specific isotope. The dashed curve is the prediction of Gibbs,[16] which appears to have underestimated the cross section and its trend with energy. Unfortunately, neither we nor Clark *et al.*[15] managed to get much information on the cross section for the coherent reaction, $^{209}\text{Bi}(p,\pi^-)^{210}\text{At}$. On the ^{210}At figure we also display (solid curve) the excitation curve[10] for the production of ^{210}Po by the corresponding (p,π^0) reaction, i.e., $^{209}\text{Bi}(p,\pi^0)^{210}\text{Po}$ along with upper limits remaining after subtraction of secondary effects. It appears that the (p,π^-) cross section is at least one order of magnitude smaller than the corresponding (p,π^0) cross section. All observed $(p,\pi^- xn)$ cross sections (σ_x) seem to rise steeply with energy right above threshold, then decrease slowly. This behavior is similar to that displayed by the (p,π^0) reaction, suggesting a possible common reaction mechanism. A peak in the excitation curve is seen several tens of MeV above threshold, mainly for the heavy isotopes (^{207}At—^{209}At). This apparent peak probably arises from the increasing relative value of the cross section for successive neutron evaporation products down to ^{204}At and disappears for lighter species. A similar peak appears for the (p,π_0) reaction product yield. Unfortunately, no data exist on the $(p,\pi^0 xn)$ reaction since the measured Po activities[13,14] represent mostly the (p,xn) reactions which have a much larger cross section.

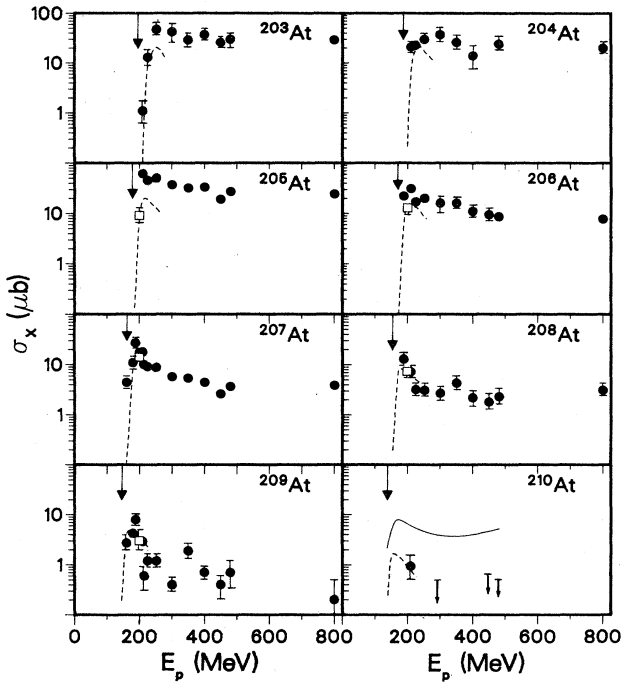

FIG. 3. Displayed here are the excitation functions from the yield of At from the series of reactions $(p,\pi^- xn)$ on ^{209}Bi corrected for contributions from secondary reactions (see the text). For ^{210}At upper limits only are indicated in many cases. The open square is the result of Clark *et al.* (Ref. 15). The dashed curve is a prediction by Gibbs (Ref. 16). The threshold for each reaction is represented by an arrow (see Table I). The ^{210}At graph also displays the excitation curve (solid line) for the $^{209}\text{Bi}(p,\pi^0)^{210}\text{Po}$ reaction (Ref. 13), along with upper limits remaining after subtraction of secondary effects.

The measured cross sections σ_x were summed up at each bombarding energy E_p to yield the observed summed cross section $\sum\sigma_x$, whose values are displayed in the second column of Table III. It should be noted that $\sum\sigma_x$ is still not σ_t, the sum of all the cross sections for the $^{209}\text{Bi}(p,\pi^- xn)^{210-x}$At reactions, since we have not included the isotopes lighter than ^{203}At, which were not observed due to their short half-lives. We then assumed that the yield distribution of astatine isotopes is Gaussian in shape and fitted the σ_x distribution at each bombarding energy E_p with a Gaussian; Table IV displays the parameters obtained from the fits. This approach for the data obtained at 480 MeV is displayed in Fig. 4. The average number of neutrons, $\bar{x}$, which corresponds to $^{210-\bar{x}}$At, is shown in the second column; the peak of the Gaussian, $\sigma_{\max}$, is shown in the third column; while the full width at half maximum (FWHM) is shown in the fourth column. For the low energy bombardments ($E_p \leq 225$ MeV), the light isotopes ($x \geq 8$), which were not observed, are not expected to contribute significantly, so that for these bom-

TABLE III. Summed cross section $\sum\sigma_x$ for the $^{209}\text{Bi}(p,\pi^- xn)^{210-x}$At reactions. The last column displays the estimated σ_t.

E_p (MeV)	$\sum\sigma_x$ (μb)	σ_t (estimated) (μb)
160		(3)
180		(15)
188	70±9	(76)
200	46±5[a]	(46)
210	143±10	(143)
215		(85)
225	112±10	(123)
252	160±14	220^{+203}_{-74}
300	141±23	195^{+72}_{-72}
350	115±13	145^{+67}_{-43}
399	102±13	150^{+32}_{-32}
450	~80	115^{+18}_{-18}
481	116±11	135^{+82}_{-30}
800	89±5	160^{+147}_{-76}

[a]Reference 15.

TABLE IV. Parameters of Gaussian fits for the distribution of $^{210-x}$At isotopes.

E_p (MeV)	$\bar{x}$ (p,π^-xn)	σ_{max} (μb)	FWHM (units of A)	$\bar{x}$ [a] (p,xn)
188	2.8±0.4			
200[b]	3.4±0.6			
210	4.4±0.3			6.0±0.2
225	4.9±0.6			
252	6.3±1.0	43.2±8.2	4.8±4.3	
300	6.4±0.4	42.6±3.2	4.3±1.5	5.4±0.1
350	6.0±0.4	31.1±3.5	4.3±1.9	
399	6.1±0.8	47.3±3.8	3.0±0.6	5.6±0.1
450	6.4±0.1	27.6±1.1	3.9±0.6	6.1±0.2
481	6.5±0.6	29.6±3.5	4.3±2.5	6.3±0.1
800	7.2±1.5	27.8±5.4	5.4±4.8	

[a]Reference 14.
[b]Reference 15.

barding energies $\bar{x}$ is the arithmetical weighted average of the observed x. The fifth column of Table IV displays the average number of neutrons emitted in the (p,xn) reactions on ^{209}Bi.[14] From Table IV wee see that for $250 \leq E_p \leq 480$ MeV, $\bar{x}$ is practically constant for both the (p,π^-xn) and the (p,xn) reactions, with $\bar{x}$ (p,π^-xn) being larger than $\bar{x}$ (p,xn) by $\approx$0.4 neutrons. We then use the results of the Gaussian fits (Table IV) to extrapolate the observed σ_x at each energy to the lighter isotopes (^{202}At and lighter) and obtain an estimate for σ_t, the sum cross section for the DCE (p,π^-xn) reaction. This estimated DCE σ_t is presented in the last column of Table III and in Fig. 5. We may have overestimated the quoted errors of σ_t in treating the uncertainties in $\bar{x}$, σ_{max}, and FWHM as independent; however, the lower limit was never taken as lower than $\sum\sigma_x$. The estimates given in parentheses in Table III are fit to the standard Gaussian curve based only on $A=209$ and 207 data. The open square is the result of Clark *et al.*[15] for $E_p=200$ MeV. The solid curve is the prediction of Long *et al.*,[17] while the dashed curve is that of Gibbs.[16] Also shown are the measured inclusive cross sections on σ_{inc}, of Crawford *et al.*[9] at $E_p=585$ (open circle), and of Cochran *et al.*[10] at $E_p=735$ MeV (open triangle). Very recent data[30] of inclusive (p,$\pi^\pm$) production on uranium obtained at TRIUMF at $E_p=330$, 400, and 500 MeV are also displayed (crosses). The total inclusive cross sections measured by Krasonov *et al.*[11] on Cu were scaled with the Cu-Pb data of Crawford *et al.*[9] at 585 MeV, and Cochran *et al.*[10] at 730 MeV, and are given by the solid triangles. The shape of the DCE σ_t excitation curve displays an increase right above threshold, as did the excitation curves for the individual σ_x, with the leveling off or even a decline after peaking at $E_p \approx 240$ MeV. Clearly, no sharp features are expected or observed for σ_t, which is a sum of cross sections with different Q values. We also note that at $E_p \approx 500$ MeV, the ratio of σ_t to the total inclusive cross section is about 0.3%.

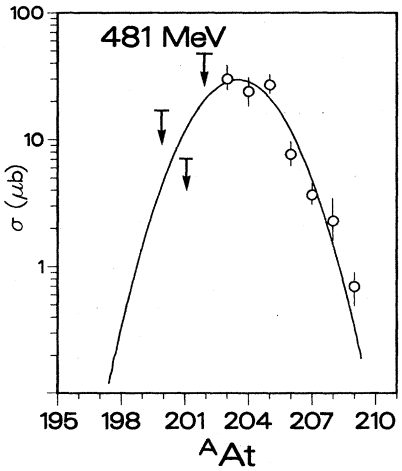

FIG. 4. The distribution as a function of astatine mass number at $E_p=481$ MeV. The solid curve is the Gaussian fit using parameters from Table IV. Upper limits for lighter nuclides were calculated from the detection limits of the data presented in Ref. 14.

IV. DISCUSSION

In an attempt to understand the main features of this study concerning individual and summed (p,π^-xn) excitation functions, the mass distributions, and the relative magnitudes of the DCE vs total inclusive cross sections, we will first draw upon the two-nucleon mechanisms

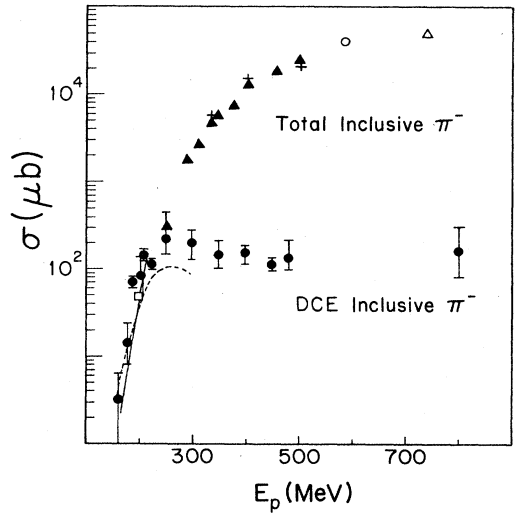

FIG. 5. Excitation curve for σ_t, the sum cross section for the ^{209}Bi(p,π^-xn)$^{210-x}$At DCE reactions as calculated from the Gaussian fits (see the text). The open square is the result of Clark *et al.* (Ref. 15). The solid and dashed curves are the predictions of Long *et al.* (Ref. 17) and Gibbs (Ref. 16), respectively. The open circle and triangle are the published experimental results of Crawford *et al.* (Ref. 9) and Cochran *et al.* (Ref. 10), respectively, for σ_{inc}, the inclusive cross section for the (p,π^-) reaction on lead. The crosses are recent unpublished results of DiGiacomo *et al.* (Ref. 30) on inclusive π^- production on uranium. The filled triangles are the scaled data from Krasonov *et al.* (Ref. 11).

(TNM) and the calculations of the ^{209}Bi(p,π) reactions by Dillig[13] and Gibbs.[16] These theories rely upon the coherent production of pions in a p_A collision so that the entire nucleus must take part in the process. The amplitudes for the reactions studied here are characterized by the emission of negative pions from target neutrons, $pn_A \rightarrow \pi^- pp_A$. Gibbs[16] has noted that within the context of a TNM the astatine products result from the incoming captured proton striking a target neutron, which in turn emits a π^-, leaving the doubly coherent product (^{210}At) in a highly excited 2p1h state that further decays by evaporating neutrons. Using the target emission model information is inferred about the original excitation spectrum from the residual isotopic distribution. Qualitatively, above the pion threshold new channels open up successively, the individual cross section rises quickly with excitation energy to about 30 MeV above threshold where no more particle stable states are populated and the cross section reaches a maximum. The major factors affecting this threshold behavior are the nuclear states density and the influence of very high-lying nucleon states as noted by Dillig[13] in the ^{209}Bi(p,π^0)^{210}Po study. The summed (p,$\pi^- x$n) excitation function follows the same general behavior in that it rises rapidly with excitation energy due mainly to improved phase space conditions until the maximum nuclear excitation occurs when the energy, momentum matching, and general phase space considerations become less favorable for trapping the proton which corresponds to approximately $E_p = 225$ MeV. The total inclusive cross section continues to increase dramatically above this energy as shown in Fig. 4, dominating π^- production as the free NN$\rightarrow$NN threshold ($E_p \sim 280$ MeV) is crossed.

In Fig. 5 the excitation curve for the summed (p,$\pi^- x$n) reaction is compared with the calculations of Gibbs[16] and Long, Sternheim, and Silbar.[17] The calculation of Ref. 17 included three contributions to the total (p,$\pi^- x$n) cross section: (a) $pn_A \rightarrow \pi^- pp_A$, (b) (p,$\pi^0$) followed by ($\pi^0$,$\pi^-$), and (c) (p,n) followed by (n,π^-). The relative magnitudes of the direct production (a) versus the two charge exchange mechanisms [(b) and (c)] are roughly equal. The predicted slope of the increasing excitation function up to $E_p = 220$ MeV exhibits good agreement with the data. Gibbs's[16] calculation of individual (p,$\pi^- x$n) yields are generally underestimated and the slope of the tails are greater than that observed experimentally, as shown in Fig. 3. However, the general energy dependence of the summed (p,$\pi^- x$n) cross section is correctly predicted to about 250 MeV. This may support an interpretation that the two-nucleon mechanism is primarily responsible for the astatine products. The slopes of the individual (p,$\pi^- x$n) cross sections are sensitive to the level density assumption, and had Gibbs[16] used the level density parameters extracted from the ^{209}Bi(p,π_0)^{210}Po study,[10] much better agreement may have been possible. The important point is that the TNM calculation[16] is in satisfactory agreement with both the excitation functions and mass yield curves for the ^{209}Bi(p,$\pi^- x$n)$^{210-x}$At reaction.

The astatine mass distribution displayed in Fig. 4 and summarized in Table IV provides important information concerning the original excitation spectrum of the nucleus within the context of the TNM following π^- emission. The average number of neutrons emitted in the (p,$\pi^- x$n) reaction for $E_p > 250$ MeV is 6.4±0.8 which yields a most probable excitation of

$$\langle E_{mp} \rangle = [\langle B_n \rangle + \langle kT \rangle](\bar{x}) \approx 60 \text{ MeV} , \quad (1)$$

where $\langle B_n \rangle$ is the average neutron separation energy taken as 8.1 MeV and kT is a smaller thermal energy. This most probable excitation yields a momentum transfer of $\langle P_{mp} \rangle = 335$ MeV/c and is consistent with other proton-nucleus studies at intermediate energies which have been examining the linear momentum transfer process.[14,31–33] The average FWHM for the (p,$\pi^- x$n) mass distribution for $E_p > 252$ MeV is 4.3±2.8 as compared with 6.6±0.5 units for the (p,xn) reaction,[14] the differences being due mainly to the momentum distribution from the initial fast interaction, followed by the statistical emission process.

In the final analysis we will perform a schematic parametric calculation based upon a phenomenological model to compare the summed (p,$\pi^- x$n) cross section (σ_t) with the total inclusive cross section (σ_{inc}) as a function of incident proton energy. By concentrating on the cross section ratio many of the complexities involved in the pion intranuclear collision can hopefully be avoided. The nucleus will be treated as a single point interaction region with all regular distributions assumed to be isotropic and averaged over all weak dependences. Independent of the specific intermediate mechanism the final state contains a π^- (which we assume escapes without depositing any energy in the nucleus) and two positive energy protons. The more energetic these protons the more likely they are to escape the interaction region. Thus our experiment samples a fairly constant tail of the final state protons. Thus, while σ_{inc} increases sharply with phase space, the apparent independence of σ_t (and $\bar{x}$) at high values of E_p reflects the fact that the formation of At occurs only for a fairly constant tail of the final state protons.

Let us suppose that a pion was produced and a total energy E_{tot} is available for distribution between the pion and the two protons. We write (letting $E_p = T_p$ for simplicity)

$$E_{tot} = E_p - m_\pi - E^* , \quad (2)$$

where E^* is the average energy deposited in the nucleus in the pion-producing interaction. Let us define $\rho(E_1,E_2;E_{tot})$ to be the normalized probability density for the two protons to have energies E_1 and E_2.

$$\int_0^{E_{tot}} \int_0^{E_{tot}} \rho(E_1,E_2;E_{tot}) dE_1 dE_2 = 1 . \quad (3)$$

Let us further define $P(E)$ as the volume-averaged probability that a proton with energy E will interact in the nucleus such that no protons (primary or secondary) would then escape since the energy would be too low to penetrate the barrier. Using the functions, thus defined, we write

$$\frac{\sigma_t}{\sigma_{inc}}(E_p) = \int_0^{E_{tot}} \int_0^{E_{tot}} \rho(E_1,E_2;E_{tot}) \times P(E_1)P(E_2) dE_1 dE_2 . \quad (4)$$

The average energy deposited in the nucleus by the

trapped protons is therefore

$$E_{\rm dep}=\frac{\sigma_{\rm inc}}{\sigma_t}\int_0^{E_{\rm tot}}\int_0^{E_{\rm tot}}\rho(E_1,E_2;E_{\rm tot})P(E_1)$$

$$\times P(E_2)(E_1+E_2)dE_1dE_2. \quad (5)$$

The total excitation energy E_x of the compound system is $E_{\rm dep}+E^*$, and is essentially proportional to $\bar{x}$; therefore,

$$\bar{x}=\frac{E_{\rm dep}+E^*}{\langle B_{\rm n}\rangle+\langle kT\rangle}\ , \quad (6)$$

where $\langle B_{\rm n}\rangle$ is an average neutron separation energy and $\langle kT\rangle$ is the (smaller) thermal energy. In fact, because elementary pion production (NN$\rightarrow$NNπ) grows very fast with available energy, we may assume that it primarily occurs when the initial proton (having undergone possibly only low momentum transfer, simple, and charge-exchange scattering) interacts with a nucleon at the top of the Fermi sea. For this case we are justified in approximating

$$E^*\approx B_{\rm n}\ .$$

In order to obtain quantitative results, explicit expressions for ρ and $P(E)$ are required. Assuming the three particles to be independent, quasifree, and correlated only by total energy conservation, we can eliminate the many complex factors which enter into a realistic evaluation of ρ. Using nonrelativistic kinematics and recalling that the phase-space volume differential goes as p^2dp or as $E^{1/2}dE$, ρ simplifies to

$$\rho(E_1,E_2;E_{\rm tot})\alpha(E_1E_2)^{1/2}$$

$$\times(E_{\rm tot}-E_1-E_2)_j(E_1+E_2)<E_{\rm tot}\ , \quad (7)$$

where the function $P(E)$ is directly related to the (p,xn) cross section at the corresponding energy. It can also, in principle, be evaluated by well-understood and quite reliable intranuclear cascade techniques. We shall only rely indirectly on such calculations to select a reasonable one-parameter functional representation of $P(E)$. Recalling that below the Coulomb barrier E_C, the escape probability is practically zero, we have

$$P(E)=1;\ \ E<E_C\ .$$

For energies above the barrier we use

$$P(E)=\exp\left[-\frac{(E-E_C)}{\omega}\right];\ \ E\geq E_C\ ,$$

where we should stress that the general behavior of the theoretical results is only mildly sensitive to the particular parametrization used. The parameter ω is monotonically related to the nucleon mean-free path (λ) in the relevant energy range, although their exact relationship is quite complicated.

The numerical results are shown in Figs. 6 and 7. In Fig. 6 the ratio of $\sigma_{\rm inc}/\sigma_t$ is plotted as a function of $E_{\rm p}$ for a number of parameter values, ω, and compared with the experimental ratios. The latter was obtained by extrapolating and interpolating values of $\sigma_{\rm inc}$. In Fig. 7 is shown a comparison of the calculated neutron yields ($\bar{x}$) with the experimental values obtained from Table IV using the same parametric set as in Fig. 6. The fact that the behavior of both quantities is reproduced rather well by the same parameter (ω) provides support for this analysis which depends strongly on general phase-space arguments.

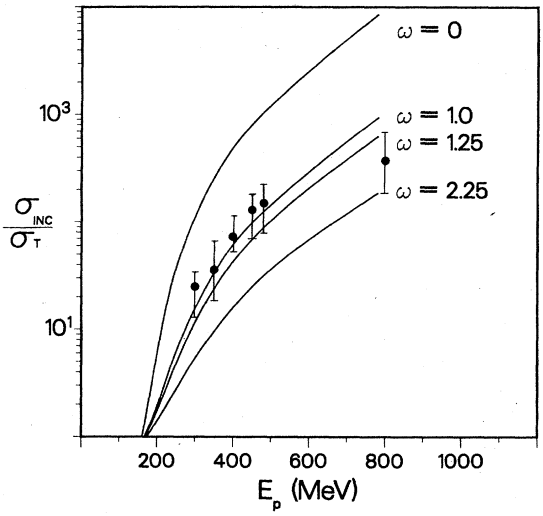

FIG. 6. The ratio $\sigma_{\rm inc}/\sigma_t$ as a function of proton energy $E_{\rm p}$, for a number of parameters ω. The experimental points were obtained by dividing extrapolated $\sigma_{\rm inc}$ by estimated values of σ_t.

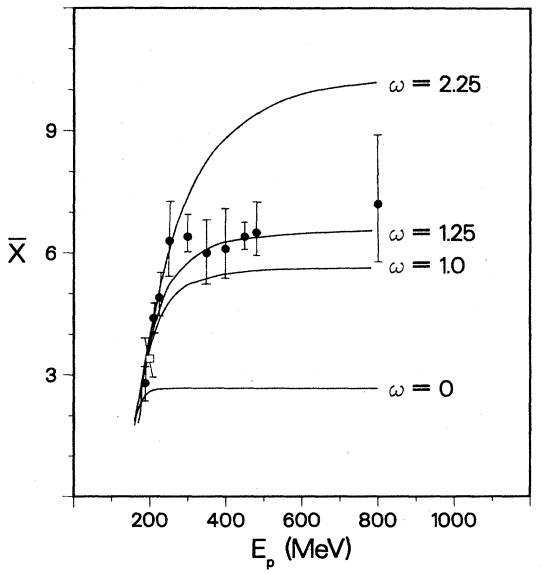

FIG. 7. Comparison of calculated and experimentally measured average neutron number $\bar{x}$ as a function of $E_{\rm p}$. The different parameter values are the same as in Fig. 6.

V. SUMMARY

The ^{209}Bi(p,π^-xn)$^{210-x}$At DCE reaction was studied using activation and radiochemical techniques in the energy region from 120 to 800 MeV. The individual astatine product excitation functions increase rapidly reaching a maximum about 30 MeV above threshold. This behavior is similar to the ^{209}Bi(p,π^0)^{210}Po excitation function measured earlier[13] and lends support to the application of a two-nucleon mechanism for these (p,π) reactions. The qualitative features of TNM calculations by Dillig[13] and Gibbs[16] are in good agreement with the data reproducing both the energy dependence and mass distribution of the (p,π_0) and (p,π^-xn) reactions, respectively. The density of states factor and high-lying nucleon states play an important role in determining the shape of the excitation curves. The (p,π^-xn) channel dominates π^- production from threshold up to about E_p=225 MeV. The ratio of σ_{inc}/σ_t was calculated from general phase-space considerations and found to be in good agreement with experiment predicting both the cross section ratio and $\bar{x}$, the average number of emitted neutrons.

These radiochemical data for products with as many as seven removed from the doubly coherent product (^{210}At) display near-Gaussian shapes for the mass distributions for all energies above 225 MeV, indicating a most probable mass residue of 203.6±0.8 or an average nuclear excitation of ≈60 MeV. The most probable momentum transfer inferred from these distributions is ≈335 MeV/c, a value in good agreement with direct measurements for proton-induced reactions.[30–32]

ACKNOWLEDGMENTS

We would like to thank the operating staff at IUCF, TRIUMF, and LAMPF for their efforts in helping to obtain stable and intense proton beams at various required energies. Theoretical discussions with M. Dillig, W. Gibbs, R. Silbar, M. Sternheim, and M. Huber were most elucidating. One of us (T.E.W.) would like to thank G. Emery and P. Singh for their help and support in the early stages of this work. B. Dropesky and G. Geisler were instrumental in obtaining the data at 800 MeV. This work was supported in part by the National Science and Engineering Research Council of Canada, the National Science Foundation (U.S.), and the Department of Energy (U.S.).

APPENDIX: CALCULATION OF YIELDS FOR SECONDARY REACTIONS

Metzger and Miller[34] expressed the thick target production cross section for secondary nuclei as

$$\sigma_{sec}=\int_0^\infty \sigma_f(E_f)P(E_f)dE_f \ , \tag{A1}$$

where $\sigma_f(E_f)$ is the angle integrated, energy dependent cross section for fragment production and $P(E_f)$ is the probability that a fragment of initial energy E_f will interact at some point in its range to form a secondary nucleus. This probability is expressed as

$$P(E_f)=N\int_0^{E_f}\sigma_c(E_f)dr_f \ , \tag{A2}$$

where N is the number of target nuclei per cubic centimeter, $\sigma_c(E_f)$ is the cross section for formation of a secondary nucleus, and dr_f is an element of the fragment range. Integration is made possible by eliminating dr_f by an appropriate range-energy relation ($-dE/dr$).

In the present work, $\sigma_c(E_f)$ in Eq. (A2) was replaced by specific (α,xn) excitation functions. These were obtained by fitting experimental data[35–37] to a semiempirical function based on a model developed by Jackson,[38,39]

$$\sigma(\alpha,xn)=\sigma_c(E_\alpha)[a(E_\alpha)^bP_{(x+1)}-c(E_\alpha)^dP_x] \ , \tag{A3}$$

where

$$\sigma_c(E_\alpha)=\pi(R+\lambda)^2\left[1-\frac{B}{E_\alpha}\right] \tag{A4}$$

and $P_{(x)}$ and $P_{(x+1)}$ refer to the probabilities of evaporating x and $(x+1)$ neutrons, respectively. The parameters a, b, c, d, and R as well as the level density parameter were varied in a least squares fitting procedure to obtain smooth curves representing the individual excitation functions for x=2–7.

The term $\sigma_f(E_f)$ in (A1) was replaced by the (p,α) angle integrated production cross section. Only alpha energies higher than 20 MeV (the threshold for ^{211}At production) were considered; the shape was approximated by the function

$$\frac{d\sigma_{(p,\alpha)}}{dE_\alpha}\left[\frac{\text{mb}}{\text{MeV}}\right]=A\exp[-B(E_\alpha-20\text{ MeV})]. \tag{A5}$$

Data on ^{209}Bi(p,α) at 90 MeV (Ref. 40) and ^{208}Pb(p,α) at 164 MeV (Ref. 41) were used to estimate a value of 0.077 MeV^{-1} for the parameter B. The parameter A is a function of proton energy and was obtained by normalizing to ^{211}At produced at each proton energy.

The range-energy relation used to transform (A2) was from Bethe,[42]

$$-\frac{dE}{dr}=\frac{4\pi e^4z^2ZN}{m_ev^2}\ln\left[\frac{2m_ev^2}{\langle I\rangle}\right] \ , \tag{A6}$$

while the average ionization potential for Bi, $\langle I\rangle$=0.763 MeV, was from Ziegler.[43]

The calculation was performed by stepwise numerical integration of (A3) and (A5). The alpha energy distribution was divided into i intervals $(dE_\alpha)_i$ of ~5 MeV width; the average energy $(\bar{E}_\alpha)_i$ and production cross section $(\bar{\sigma}_{(p,\alpha)})_i$ in each interval were then calculated. The target thickness was likewise divided into j intervals $(d_r)_j$ and the energy of a particular α_i in each interval $(\bar{E}_j)$ calculated from the stopping power formula. The probability of the alpha interacting in a particular thickness interval was taken as the product of the number of target nuclei in the interval (n_j), and the (α,xn) cross section at that alpha energy, $\sigma(\bar{E}_j)_{(\alpha,xn)}$. The total probability of the alpha interacting with the target was described by

$$P_i=1-\exp\left[-\sum_j n_j\sigma(\bar{E}_j)_{(\alpha,xn)}\right] \ . \tag{A7}$$

The total production cross section for a particular astatine nuclide from alphas of all energies was,

$$\sigma_{\text{sec}} = \sum_i (\bar{\sigma}_{(p,\alpha)})_i P_i \ . \quad \text{(A8)}$$

Since secondary production in thin targets is a fraction of the thick target production, all calculations were normalized to the experimentally observed yield of ^{211}AT (produced only by secondaries); this was accomplished by two methods. In the first, the parameter A was varied to bring the calculation into agreement with the ^{211}At yield at each proton energy. This value was then used in the calculation of all other secondary production yields. The second method used values of A extracted from thick target experiments[23–29] and normalized to the ^{211}At yield by determining an "effective" target thickness. This effective thickness, in essence, was averaged over all alpha emission angles (and was used in calculating subsequent secondary yields). The results of the two calculations were identical. The yields of At nuclides produced by (^{3}He,xn) secondary reactions were calculated in an analogous manner and amounted to $\sim 10\%$ of the alpha induced yields.

*Permanent address: General Physics Corporation, 10650 Hickory Ridge Rd., Columbia, MD 21044.

[1]D. F. Measday and G. A. Miller, Annu. Rev. Nucl. Part. Sci. **29**, 121 (1979).
[2]B. Höistad, Adv. Nucl. Phys. **11**, 135 (1978)
[3]M. Dillig, Nucl. Phys. **A335**, 407 (1980).
[4]H. W. Fearing, TRIUMF Report TRI-80-3, 1980.
[5]*Pion Production and Absorption in Nuclei—1981 (Indiana University Cyclotron Facility),* Proceedings of the Workshop on Pion Production and Absorption in Nuclei, AIP Conf. Proc. No. 79, edited by R. D. Bent (AIP, New York, 1981).
[6]W. O. Lock and D. F. Measday, *Intermediate Energy Nuclear Physics* (Methuen, London, 1970), Chap. 8.
[7]J. M. Eisenberg and D. S. Kolton, *Theory of Meson Interactions with Nuclei* (Wiley-Interscience, New York, 1980).
[8]S. E. Vigdor, T. G. Throwe, H. C. Green, W. W. Jacobs, R. D. Bent, J. J. Kehayias, W. K. Pitts, and T. E. Ward, Nucl. Phys. **A396**, 610 (1983).
[9]J. F. Crawford, M. Daum, G. H. Eaton, R. Frosch, H. Hurschmann, R. Hess, and D. Warren, Phys. Rev. C **22**, 1184 (1980).
[10]D. R. F. Cochran, P. N. Dean, P. A. M. Gram, E. A. Knapp, E. R. Martin, D. E. Nagle, R. B. Perkins, W. J. Shlaer, H. A. Thiessen, and E. D. Theriot, Phys. Rev. D **11**, 3085 (1972).
[11]V. A. Krasonov, A. B. Kurepin, A. I. Reshetin, K. O. Oganesjan, and E. A. Pasyuk, Phys. Lett. **100B**, 11 (1982).
[12]J. Julien *et al.*, Phys. Lett. **142B**, 340 (1984).
[13]T. E. Ward, P. P. Singh, D. L. Friesel, A. Yavin, A. Doron, J. M. D'Auria, G. Sheffer, and M. Dillig, Phys. Rev. C **24**, 588 (1981).
[14]J. M. D'Auria, M. Dombsky, G. Sheffer, T. E. Ward, H. J. Karwowski, A. I. Yavin, and J. Clark, Phys. Rev. C **30**, 236 (1984).
[15]J. L. Clark, P. E. Haustein, T. J. Ruth, J. Hudis, and A. A. Caretto, Jr., Phys. Rev. C **26**, 2073 (1982).
[16]W. R. Gibbs, Ref. 5, p. 297.
[17]D. G. Long, M. M. Sternheim, and R. R. Silbar, Phys. Rev. C **26**, 586 (1982).
[18]J. B. Cumming, Annu. Rev. Nucl. Sci. **13**, 261 (1963); A. Poskanzer, J. B. Cumming, and R. Wolfgang, Phys. Rev. **129**, 374 (1963).
[19]*Table of Isotopes,* 7th ed., edited by C. M. Lederer and V. Shirley (Wiley, New York, 1978).
[20]M. Bochvarova, Do Kim Tyung, I. Dudova, Yu. V. Norseev, and V. A. Khalin, Radiokhimiya **14**, 858 (1972).
[21]R. Gunnink and J. B. Niday, University of California Radiation Laboratory Report UCRL 51061, 1972, Vol. I.
[22]R. E. L. Green and R. G. Korteling, Phys. Rev. C **22**, 1594 (1980).
[23]E. N. Vol'nin, A. A. Vorob'ev, and D. M. Seliverstov, Zh. Eksp. Teor. Fiz. Pis'ma Red. **19**, 691 (1974) [Sov. Phys.—JETP Lett. **19**, 357 (1974)].
[24]B. V. Kurchatov, V. N. Mekhedov, L. V. Chistiakov, M. Ya. Kuznetsova, N. I. Borisova, and V. G. Solov'ev, Zh. Eksp. Teor. Fiz. **35**, 56 (1958) [Sov. Phys.—JETP **35**, 40 (1959)].
[25]Wang Yung-Yu, V. V. Kusnetsov, M. Ya. Kuznetsova, and V. A. Khalkin, Zh. Eksp. Teor. Fiz. **39**, 230 (1960) [Sov. Phys.—JETP **12**, 166 (1961)].
[26]Li Chung Hi, N. S. Mal'tseva, and V. N. Mekhedov, Yad. Fiz. **14**, 484 (1971) [Sov. J. Nucl. Phys. **14**, 272 (1972)].
[27]M. Lefort, G. Simonoff, and X. Tarrago, Nucl. Phys. **19**, 173 (1960).
[28]M. Lefort and X. Tarrago, Nucl. Phys. **39**, 447 (1962).
[29]M. Lefort and X. Tarrago, Nucl. Phys. **46**, 161 (1963).
[30]N. J. DiGiacomo, M. R. Glover, R. M. DeVries, J. C. Dousse, J. S. Kapustinsky, P. L. McGaughey, W. E. Sondheim, J. W. Sumer, M. Buenerd, and D. Lebrum, Los Alamos Laboratory Report LA-UR-84-1553, 1984 (unpublished).
[31]G. Mathews, B. G. Glagola, R. A. Moyle, and V. E. Viola, Jr., Phys. Rev. C **25**, 2181 (1982).
[32]F. Saint Laurent *et al.*, Phys. Lett. **110B**, 372 (1982).
[33]L. Woo, K. Kwiatkowski, and V. E. Viola, Jr., Phys. Lett. **132B**, 283 (1983).
[34]A. E. Metzger and J. M. Miller, Phys. Rev. **113**, 1125 (1959).
[35]J. D. Stickler and K. J. Hofstetter, Phys. Rev. C **9**, 1064 (1974).
[36]E. L. Kelly and E. Segre, Phys. Rev. **75**, 999 (1949).
[37]G. Deconninck and M. Longrie, Ann. Soc. Sci. Bruxelles, Ser. 1 **88**, 347 (1974).
[38]J. D. Jackson, Can. J. Phys. **34**, 767 (1956).
[39]M. Lefort, *Nuclear Chemistry* (Van Nostrand, London, 1968).
[40]J. R. Wu, C. C. Chang, and H. D. Holmgren, Phys. Rev. C **19**, 698 (1979).
[41]R. E. Segel, T. Chen, L. L. Rutledge, Jr., J. V. Maher, J. Wiggins, P. P. Singh, and P. T. Debeue, communication to J. L. Clark.
[42]H. A. Bethe, Z. Phys. **76**, 293 (1932).
[43]J. F. Ziegler, Nucl. Instrum. Methods **168**, 17 (1980).
[44]A. H. Wapstra and K. Box, At. Data Nucl. Data Tables **19**, 175 (1977).